Acta Cryst C STRUCTURAL CHEMISTRY
ISSN 2053-2296

Structural investigations into a new polymorph of F_4TCNQ: towards enhanced semiconductor properties

Natalie T. Johnson, Michael R. Probert and Paul G. Waddell*

Chemistry, School of Natural and Environmental Sciences, Newcastle University, Bedson Building, Edward's Walk, Newcastle Upon Tyne NE1 7RU, UK. *Correspondence e-mail: paul.waddell@ncl.ac.uk

Received 6 April 2021
Accepted 17 June 2021

Edited by A. Lemmerer, University of the Witwatersrand, South Africa

Keywords: polymorphism; F_4TCNQ; charge transfer; pairwise interaction energies; crystal structure; semiconductor; quinodimethane.

CCDC references: 2090530; 2090529; 2090528

Supporting information: this article has supporting information at journals.iucr.org/c

During the course of research into the structure of 2,3,5,6-tetrafluoro-7,7,8,8-tetracyanoquinodimethane (F_4TCNQ), $C_{12}F_4N_4$, an important compound in charge-transfer and organic semiconductor research, a previously unreported polymorph of F_4TCNQ was grown concomitantly with the known polymorph from a saturated solution of dichloromethane. The structure was elucidated using single-crystal X-ray diffraction and it was found that the new polymorph packs with molecules in parallel layers, in a similar manner to the layered structure of F_2TCNQ. The structure was analysed using Hirshfeld surface analysis, fingerprint plots and pairwise interaction energies, and compared to existing data. The structure of a toluene solvate of F_4TCNQ is also reported.

1. Introduction

2,3,5,6-Tetrafluoro-7,7,8,8-tetracyanoquinodimethane (F_4TCNQ; Fig. 1) was first characterized using X-ray crystallography by Emge *et al.* (1981) [Cambridge Structural Database (CSD; Version 5.41 of November 2019; Groom *et al.*, 2016) refcode BAKPAE] and has been reported as both a homomolecular structure (BAKPAE01–03; Krupskaya *et al.*, 2015; Salzillo *et al.*, 2016; Shukla *et al.*, 2019) and the coformer in various cocrystals, with 229 instances of such cocrystals in the CSD. F_4TCNQ is of particular interest to materials scientists given its high electron affinity (Gao & Kahn, 2001) and stable anionic form, which make it suitable for use as a p-type dopant for a range of semiconductors (Gao & Kahn, 2001; Pingel *et al.*, 2012; Cochran *et al.*, 2014). These properties have also given rise to the use of F_4TCNQ as an electron acceptor in charge-transfer complexes (Sutton *et al.*, 2016; Hu *et al.*, 2017; Fujii & Yamakado, 2018).

The family of F_nTCNQ compounds (n = 0, 2, 4) was identified as an important series of molecules for the understanding of electron transport in crystals, due to the differences in electronic properties across the series of similar molecules (Krupskaya *et al.*, 2015). While F_4TCNQ (n = 4) and TCNQ (n = 0) were found to have low electron mobility (0.1 and 0.2 $cm^2 V^{-1} s^{-1}$ at room temperature, respectively), F_2TCNQ (2,5-difluoro-7,7,8,8-tetracyanoquinodimethane, $C_{12}H_2F_2N_4$; Fig. 1) was found to have a much higher electron mobility of 6–7 $cm^2 V^{-1} s^{-1}$ at room temperature (and up to 25 $cm^2 V^{-1} s^{-1}$ at 150 K). Band-like electron transport, where the electron mobility increases upon lowering the temperature, has been observed in F_2TCNQ but not in the other compounds.

Krupskaya *et al.* (2015) postulated that the difference in the crystal structures of the compounds could be the cause of the difference in electron mobility across the F_nTCNQ family.

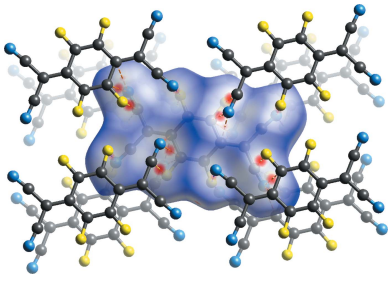

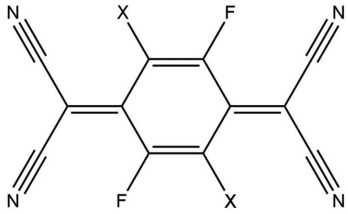

Figure 1
The structure of F_nTCNQ, where X = H for F_2TCNQ and X = F for 2,3,5,6-tetrafluoro-7,7,8,8-tetracyanoquinodimethane (F_4TCNQ)

Solid-state structure is extremely important for electron mobility (Wang *et al.*, 2012; Coropceanu *et al.*, 2007) and F_2TCNQ has a markedly different structure to the other members of the family. In F_2TCNQ (BERZON03; Krupskaya *et al.*, 2015), the molecules pack in a layered structure with molecules in adjacent (010) layers coplanar with each other (Fig. 2). This is different to that of the reported structure of F_4TCNQ (BAKPAE03; Shukla *et al.*, 2019), where the molecules are packed in a herringbone manner (Fig. 3).

Further study of this family of compounds also attributed the high electron mobility of F_2TCNQ to its crystal structure (Chernyshov *et al.*, 2017; Sosorev, 2017; Ji *et al.*, 2018; Sosorev *et al.*, 2018). According to these studies, electron motility in the solid state is affected by the number of molecules in the reduced unit cell of the crystal structure, with lower values prohibiting intermolecular vibrations according to the rigid molecule approximation (Sosorev *et al.*, 2019). The absence of these modes results in a weakening of the electron–phonon interaction; a smaller electron–phonon interaction can indicate a lesser degree of charge localization in the structure, and hence greater electron mobility (Chernyshov *et al.*, 2017). As F_2TCNQ crystallizes with one molecule in its reduced unit cell (compared to two and four molecules in those of TCNQ and F_4TCNQ), it can be expected to exhibit greater electron motility as a result.

Raman spectroscopy has been used to investigate electron–phonon interactions in the crystal structure, where charge mobility has been shown to be related to the value of the lowest vibrational frequency mode (Fratini *et al.*, 2016). The lowest vibrational mode for F_2TCNQ was found to be almost double the values for TCNQ and F_4TCNQ (polymorph I) (Chernyshov *et al.*, 2017; Sosorev *et al.*, 2018). Theoretical calculations have shown F_2TCNQ to have a three-dimensional charge carrier network (Ji *et al.*, 2018; Sosorev, 2017), which is attributed to its high charge mobility and band-like electron transport, while for F_4TCNQ and TCNQ, the charge mobility is hindered by the molecular structure and strong thermal disorder.

In the process of growing high-quality single crystals of F_4TCNQ, an additional polymorph of F_4TCNQ (polymorph II) was found that exhibits a layered structure similar to the structure of F_2TCNQ. The structure of this new polymorph was measured using single-crystal X-ray diffraction and compared to the known structures of F_4TCNQ using Hirshfeld surface analysis, fingerprint plots and pairwise interaction energies. The structure is also compared to the previously published structure of F_2TCNQ (BERZON03; Krupskaya *et al.*, 2015), as the data were measured at 100 K, the same temperature as the F_4TCNQ studies reported herein. When crystallized from toluene, a toluene–F_4TCNQ solvate was obtained, the structure of which is also presented.

2. Experimental

2.1. Crystallization

F_4TCNQ was purchased from Apollo Scientific as a solid with 97% purity and was used without further purification. Crystals suitable for single-crystal X-ray diffraction were grown *via* slow evaporation of the solvent from solutions of the compound in acetonitrile, dichloromethane (DCM) and toluene. All crystal formation took place within 24–48 h.

The crystals of F_4TCNQ grown from saturated solutions of both acetonitrile and DCM were found to be homomolecular. Crystallization from acetonitrile yielded only crystals of the previously reported structure (polymorph I), which form as yellow crystals with a regular block-like morphology, whereas in DCM, single crystals exhibiting two different morphologies were observed to form concomitantly, *i.e.* cubic crystals of polymorph I alongside octahedral crystals (Fig. 4). The octahedral crystals are the same yellow colour as those of poly-

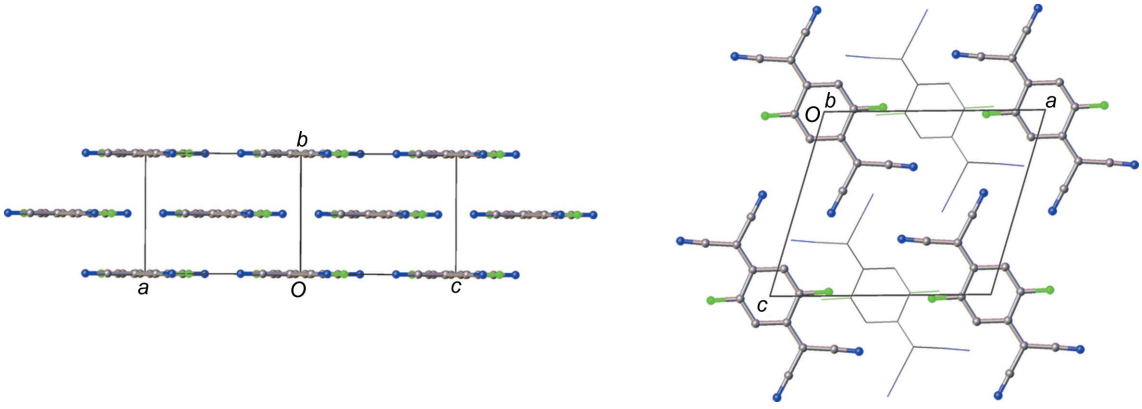

Figure 2
The structure of F_2TCNQ (CSD refcode BERZON03; Krupskaya *et al.*, 2015) highlighting the relationship between molecules in adjacent layers.

Table 1
Experimental details.

	F_4TCNQ polymorph I	F_4TCNQ polymorph II	F_4TCNQ–toluene solvate
Crystal data			
Chemical formula	$C_{12}F_4N_4$	$C_{12}F_4N_4$	$C_{12}F_4N_4{\cdot}C_7H_8$
M_r	276.16	276.16	368.29
Crystal system, space group	Orthorhombic, *Pbca*	Orthorhombic, *Pnnm*	Monoclinic, $P2_1/c$
Temperature (K)	100	100	150
a, b, c (Å)	9.1799 (3), 8.0482 (3), 14.5541 (5)	7.5140 (4), 11.6787 (6), 5.9347 (3)	8.1314 (2), 7.4141 (2), 13.6796 (4)
α, β, γ (°)	90, 90, 90	90, 90, 90	90, 100.551 (3), 90
V (Å^3)	1075.28 (6)	520.79 (5)	810.76 (4)
Z	4	2	2
Radiation type	Ag $K\alpha$, λ = 0.56086 Å	Ag $K\alpha$, λ = 0.56086 Å	Cu $K\alpha$
μ (mm^{-1})	0.09	0.10	1.09
Crystal size (mm)	0.28 × 0.22 × 0.16	0.3 × 0.17 × 0.12	0.41 × 0.05 × 0.03
Data collection			
Diffractometer	Bruker Photon II CPAD	Bruker Photon II CPAD	Rigaku OD Xcalibur Atlas Gemini ultra
Absorption correction	Numerical (*SADABS*; Bruker, 2016)	Numerical (*SADABS*; Bruker, 2016)	Analytical [*CrysAlis PRO* (Rigaku OD, 2015), based on expressions derived by Clark & Reid (1995)]
T_{min}, T_{max}	0.919, 0.982	0.931, 0.974	0.806, 0.975
No. of measured, independent and observed [$I > 2\sigma(I)$] reflections	189710, 5103, 4271	115983, 2628, 2285	10970, 1433, 1194
R_{int}	0.043	0.043	0.045
(sin $\theta/\lambda)_{max}$ (Å^{-1})	1.043	1.043	0.597
Refinement			
$R[F^2 > 2\sigma(F^2)]$, $wR(F^2)$, S	0.034, 0.115, 1.09	0.031, 0.111, 1.07	0.039, 0.109, 1.08
No. of reflections	5103	2628	1433
No. of parameters	91	61	155
No. of restraints	0	0	161
H-atom treatment	–	–	H-atom parameters constrained
$\Delta\rho_{max}$, $\Delta\rho_{min}$ (e Å^{-3})	0.75, −0.33	0.77, −0.26	0.44, −0.21

Computer programs: *APEX2* (Bruker, 2009), *CrysAlis PRO* (Rigaku OD, 2015), *SAINT* (Bruker, 2009), *SHELXT* (Sheldrick, 2015*a*), *SHELXL2014* (Sheldrick, 2015*b*), *OLEX2* (Dolomanov *et al.*, 2009) and *XPREP* (Bruker, 2009).

morph I but yield a drastically different crystal structure (polymorph II).

F_4TCNQ crystallizes from toluene as a toluene–F_4TCNQ solvate in the form of red needles.

2.2. Data collection

Crystals of polymorphs I and II and the toluene solvate were analysed using single-crystal X-ray diffraction. The crystal of polymorph I selected was grown from a saturated solution of acetonitrile, which produced larger and more abundant crystals of this polymorph than were observed in similar DCM solutions. Although the structure of polymorph I has been elucidated previously at 100 K (Shukla *et al.*, 2019), the structure was redetermined in a manner more consistent with the data collection for polymorph II to allow for a more direct comparison between the two structures.

Crystals of polymorphs I and II were cooled slowly to 100 K at a rate of 1 K min^{-1} using an Oxford Cryosystems N_2 cryostream cooler on a Bruker D8 Venture diffractometer. X-rays were generated using an Incoatec IμS 3.0 Ag source (Ag $K\alpha$, λ = 0.56086 Å). The data collected were prone to

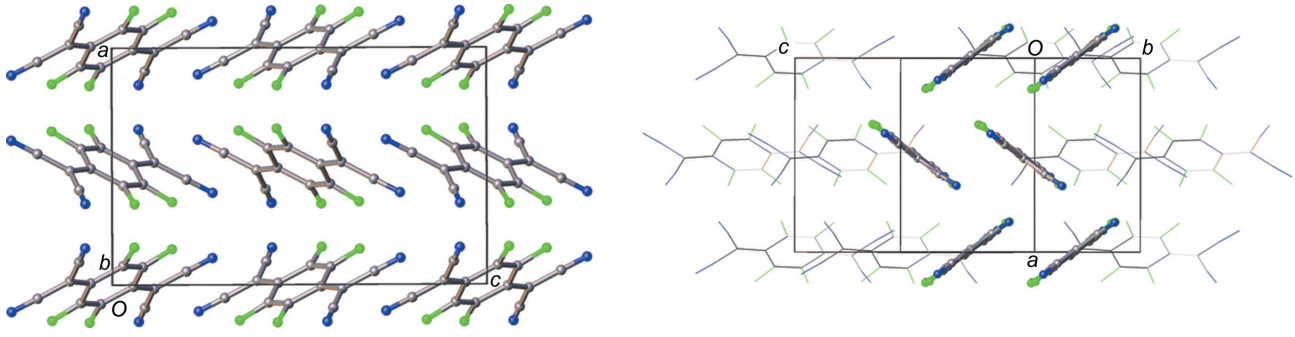

Figure 3
The structure of F_4TCNQ polymorph I, highlighting the relationship between molecules in adjacent layers (left) and the herringbone arrangement of molecules along [100] (right).

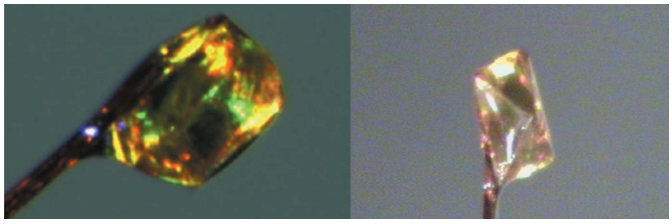

Figure 4
A crystal of F_4TCNQ polymorph I as mounted on the diffractometer (left). The octahedral crystal of F_4TCNQ polymorph II (right).

white radiation contamination (as described in Storm *et al.*, 2004); therefore, a 150 µm aluminium filter was included to remove this white radiation before the beam impinged on the sample (Macchi *et al.*, 2011). The diffraction pattern was measured on a Photon II CPAD detector using the shutterless operation mode with a sample-to-detector distance of 65 mm.

A crystal of F_4TCNQ–toluene was measured using Cu radiation (Cu $K\alpha$, $\lambda = 1.54184$ Å) at 150 K on a Rigaku Oxford Diffraction Xcalibur Atlas Gemini diffractometer equipped with an Oxford Cryosystems N_2 open-flow cooling device.

2.3. Refinement

Crystal data, data collection and structure refinement details are summarized in Table 1. H atoms were placed with idealized geometry, with U_{iso}(H) values constrained to be an appropriate multiple of the U_{eq} value of the parent atom. In the toluene solvent structure of F4TCNQ, the toluene molecule has been modelled as disordered over two sites across a centre of symmetry. The occupancies of the two parts were constrained to be 0.5 and the atomic displacement parameters were restrained. The geometry of the toluene molecule was also restrained.

3. Results and discussion

3.1. Comparison of F_4TCNQ polymorphs

Table 1 shows a summary of the experimental details for the crystallographic data from polymorphs I and II and the toluene solvate. Both forms of F_4TCNQ are very stable under ambient conditions; over a period of six months, no interconversion was observed between forms. Both polymorphs crystallize in the orthorhombic crystal system and centrosymmetric space groups. The atoms in F_4TCNQ in polymorph II sit on special positions in the unit cell, effectively a horizontal mirror plane, thereby halving the number of atoms in the asymmetric unit relative to polymorph I.

The molecular geometry of F_4TCNQ is almost identical in polymorphs I and II (with no statistically different bond lengths or angles). This is unsurprising owing to the planarity and conformational inflexibility of F_4TCNQ that is due to the high degree of conjugation within the molecule. However, despite their similar molecular structures, the packing of the molecules in the two crystal structures is markedly different.

The F_4TNCQ molecules in polymorph II are arranged to form layers coplanar with the crystallographic [001] plane and,

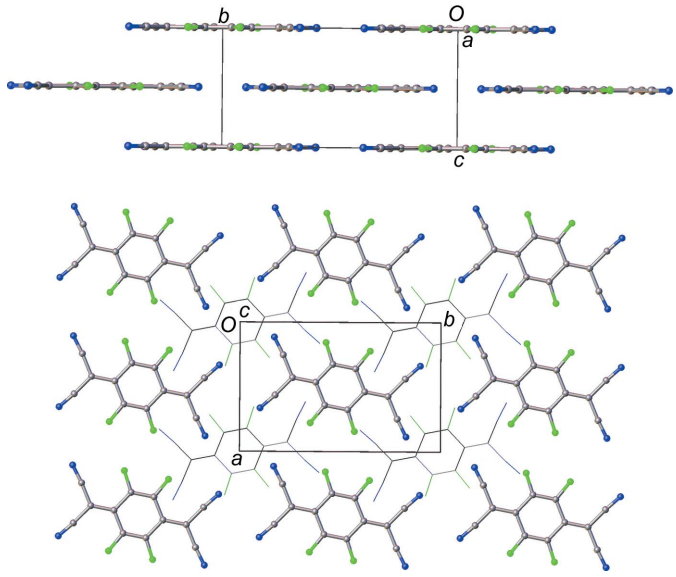

Figure 5
View down the [100] (top) and [001] (bottom) crystallographic planes of F_4TCNQ polymorph II.

as a result, the molecules in each layer are arranged coplanar to those in adjacent layers (Fig. 5) at a coplanar distance of *ca* 2.98 Å. Within a layer, the molecules are related by crystallographic translations in the [100] and [010] directions. The orientation of the molecules in adjacent layers alternates with respect to the previous layer in a manner consistent with the symmetry of the *n*-glides in the [101] and [011] directions.

Layers of molecules can also be seen in polymorph I, but the molecules are not arranged coplanar to each other. In this case, the molecules within the structure can be described as packing in a herringbone pattern, as illustrated in Fig. 3, an alternative view of the crystal structure along the [011] plane.

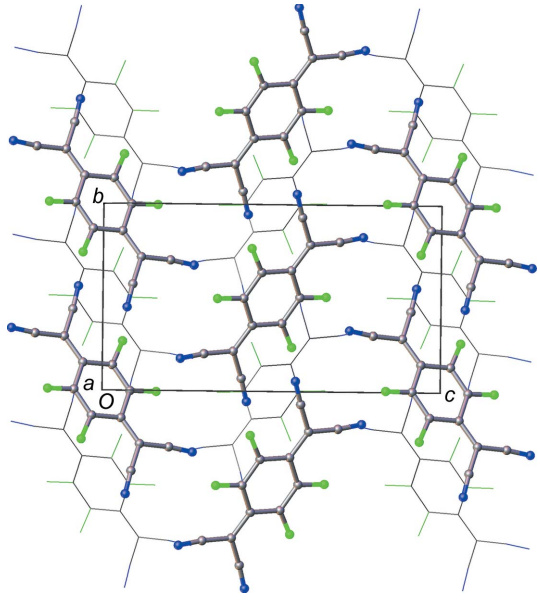

Figure 6
A view of polymorph I with adjacent layers visible in the [100] direction.

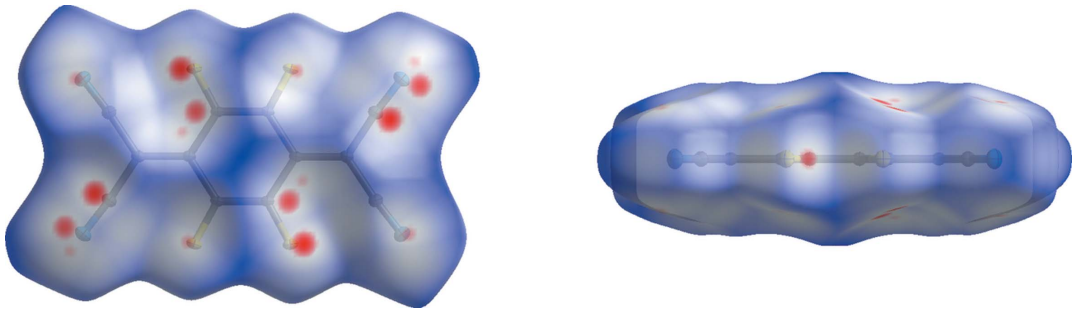

Figure 7
Hirshfeld surface calculated for a molecule of F_4TCNQ in polymorph II.

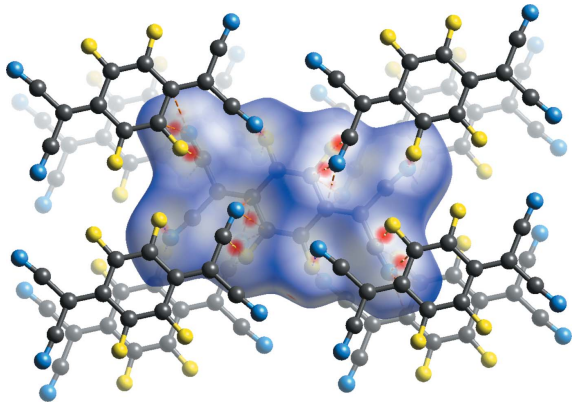

Figure 8
Hirshfeld surface of polymorph II, showing close contacts between atoms in adjacent layers, with adjacent molecules shown.

Adjacent molecules, drawn using a wireframe model, are also arranged in a herringbone formation, but at 90° to the herringbone chain highlighted in the figure. Along the [100] direction in Fig. 6, molecules are arranged in alternating orientations, which also form a herringbone motif.

3.2. Hirshfeld surfaces

Hirshfeld surfaces were calculated for the two polymorphs (Spackman & Jayatilaka, 2009; McKinnon *et al.*, 2007). The normalized distance (d_{norm}) between the closest external and internal atoms to any point on the surface is represented by the colour on the surface. A pair of atoms with d_{norm} less than the van der Waals radius of the atoms is shown in red and could indicate a close contact between those two atoms. These close contacts are important as they could indicate favourable interactions within the crystal, which could direct the packing of the molecules in the structure or influence the properties of the crystal (Bernstein, 1993).

The surface for polymorph II (Fig. 7) indicates that the majority of close contacts occur between molecules in adjacent layers. These occur in two different motifs: motif 1 between pairs of C···F and C···N interactions corresponding to close contacts between the atoms of the C—F bond of one molecule and those of the C≡N group of an adjacent molecule in

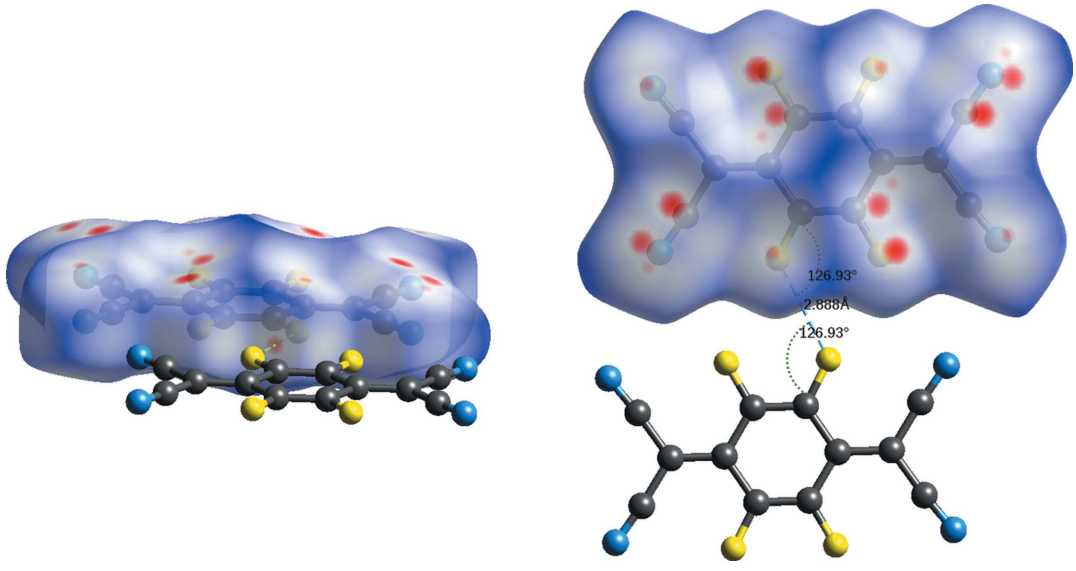

Figure 9
Hirshfeld surface of polymorph II, showing close contacts between atoms in the same layer, with adjacent molecules shown.

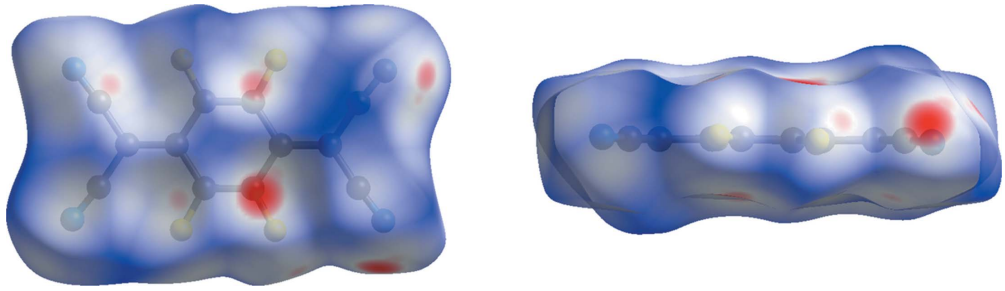

Figure 10
The Hirshfeld surface of polymorph I.

another layer (the atoms involved in this motif produce the most prominent red spots on the Hirshfeld surface), with a distance of 3.1197 (2) Å between the centroids of these two bonds; and motif 2 between only the terminal atoms of the aforementioned bonds, with the N and F atoms (Fig. 8) at a distance of 2.9885 (2) Å. Half of the C≡N and C—F atoms in a molecule exhibit close contacts of motif 1 only and the other half exhibit motif 2 only, with the same pattern of close contacts observed to form to both adjacent layers.

The arrangement of the atoms of motif 1 form a four-membered ring of close contacts. There are only four other non-organometallic structures in the CSD that contain this motif of close contacts (Wiscons *et al.*, 2018; Fan & Yan, 2014; Ishida *et al.*, 2014; Sutton *et al.*, 2016). Two of these also contain F_4TCNQ, and the motif occurs only between F_4TCNQ molecules in the structure (Wiscons *et al.*, 2018; Sutton *et al.*, 2016).

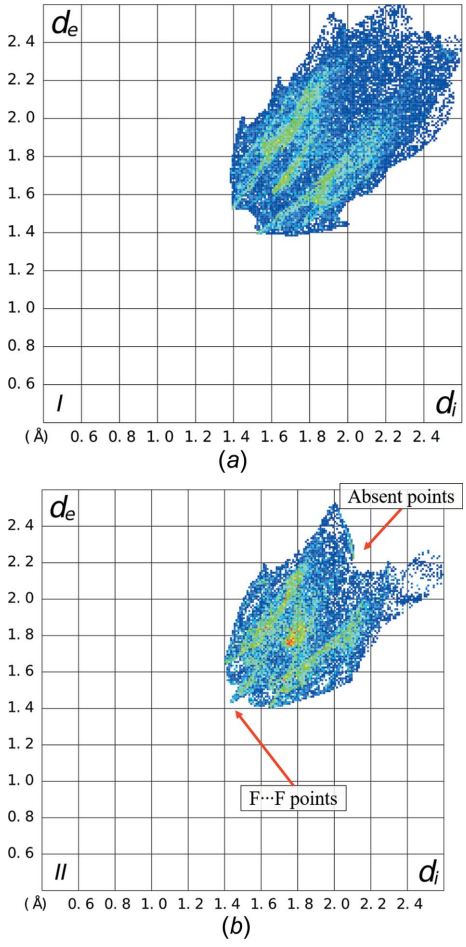

Figure 11
Fingerprint plots for polymorphs I and II.

There is only one type of close contact between molecules in the same layer, which forms between two F atoms in adjacent molecules (Fig. 9), with a distance of 2.8881 (7) Å, which is within the sum of the van der Waals radii (Alvarez, 2013). This is observed for two of the four F atoms in the molecule. Halogen bonding rules would suggest that this is a type-II contact, occurring because of the proximity of the F atoms in the structure, rather than due to the formation of a stabilizing/favourable interaction (Metrangolo & Resnati, 2013).

In contrast, there are fewer close contacts between molecules in polymorph I [22 *versus* 34 from one molecule, when totalled from those identified by *Mercury* (Macrae *et al.*, 2020)]. Most of the close contacts observed in polymorph II are not present in this arrangement – except for the F···N (motif 2) close contact (Fig. 10, and Fig. S1 in the supporting information shows the close contacts with adjacent molecules).

3.3. Fingerprint plots

Fingerprint plots (Spackman & McKinnon, 2002) result from the calculation of the distance to the closest internal and external atom for each point on the Hirshfeld surface, with the values displayed graphically. They have been used to compare polymorph structures by highlighting differences in the closest atomic contacts in the structures (McKinnon *et al.*, 2007). Those created for polymorphs I and II (Fig. 11) further illustrate the differences in packing between the two forms. In polymorph II, there are some additional points along the diagonal of the graph at short distances, which are a result of like–like F···F contacts, contacts between equivalent F atoms externally and internally of the Hirshfeld surface. In polymorph I, F atoms in adjacent molecules do not approach as closely as observed in polymorph II. This is evident in Fig. S2 (see supporting information), a version of the fingerprint plots where only points relating to F···F contacts are displayed in colour.

3.4. Energy comparisons

To further compare polymorphs, pairwise interaction energies were calculated using *CrystalExplorer* (Turner *et al.*, 2014,

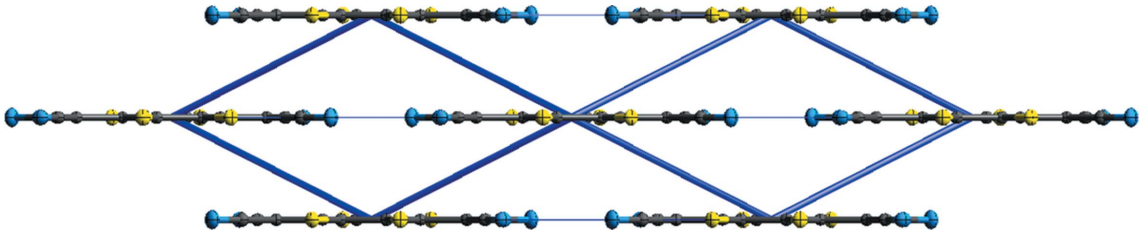

Figure 12
Energy framework for polymorph II of F_4TCNQ calculated using *CrystalExplorer17.5*. The lines between molecules indicate the relative size of the pairwise energies between molecules. E_{tot} between molecules in adjacent layers are calculated as −33.3 kJ mol^{-1}.

2017). As both polymorphs form concomitantly in DCM, but only polymorph I has been reported in the literature, there may be an energetic preference for one polymorph over another. Pairwise interaction energies were calculated for a central molecule to surrounding molecules within a radius of 3.8 Å and consist of scaled values for electrostatic, repulsive, polarization and dispersion contributions to the total interaction energy (E_{tot}) using the [B3LYP/6-31G(d,p)] energy model. The tables of values are included in the supporting information (Tables S2 and S3). These values can be used to compute an approximate average energy of the structure, and thus indicate if one polymorph is more stable than another. Energy frameworks for F_4TCNQ polymorph I and F_2TCNQ have been discussed previously by Shukla *et al.* (2019).

For polymorph II, there are three different molecule pairs – one from the central molecule to molecules in adjacent layers, and two from molecules within the layers. The energy frameworks created from the calculations show that the largest E_{tot}, −33.3 kJ mol^{-1}, is calculated between molecules in adjacent layers (Fig. 12). This value is much larger than the contributions between atoms in the same layers, which are less than −5 kJ mol^{-1}. Within the layers, there are two different pairs of interactions (Fig. 13) – those that form close F···F contacts between molecules and those that do not. Both pairs having positive electrostatic energies, indicating destabilizing contributions from electrostatic interactions. It is interesting to note that the molecules within the layers that have close F···F contacts are calculated as having an overall stabilizing interaction, albeit small (−1.1 kJ mol^{-1}), despite the positive electrostatic energy.

In polymorph I, the interaction energies have less variation. Fig. 14 shows a view of the energy framework for E_{tot}. The largest negative values of E_{tot} are found for molecules in the same herringbone chain, with the greatest overall being for molecules that are also in the same layer (−34.0 kJ mol^{-1}). This value is the largest calculated E_{tot} of the two polymorphs. Smaller E_{tot} values are calculated between the other surrounding molecules. All pairs of molecules have negative calculated electrostatic energies, E_{ele}.

If mean pairwise energies are calculated by averaging the contributions of the surrounding molecules, we obtain values of −17.85 and −23.03 kJ mol^{-1} for polymorphs I and II, respectively (Equation S1 in the supporting information). These values are similar in energy, which is expected in concomitant polymorphism. It is interesting to note that the unreported polymorph II is lower in energy and likely the thermodynamic polymorph, which raises the question of why it has not been reported previously.

Crystallization conditions have been shown to play a role in polymorph formation (Bernstein & Bernstein, 2002; Isakov *et al.*, 2013; Tran *et al.*, 2012). In the previous reported structures of F_4TCNQ polymorph I that were deposited in the CSD, crystals were grown using vapour transport (Krupskaya *et al.*, 2015), solution growth (Salzillo *et al.*, 2016), sublimation (Shukla *et al.*, 2019) and from a solution of acetonitrile (Emge *et al.*, 1981). The growth of only polymorph I from recrystallizations with acetonitrile could suggest an interaction

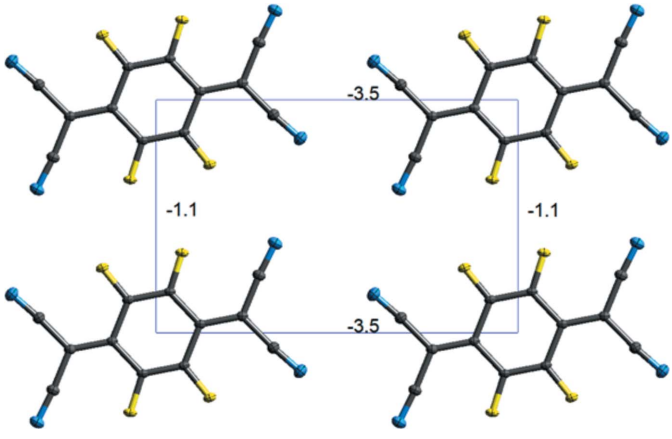

Figure 13
Energy framework for molecules within a layer of polymorph II of F_4TCNQ, calculated using *CrystalExplorer17.5*.

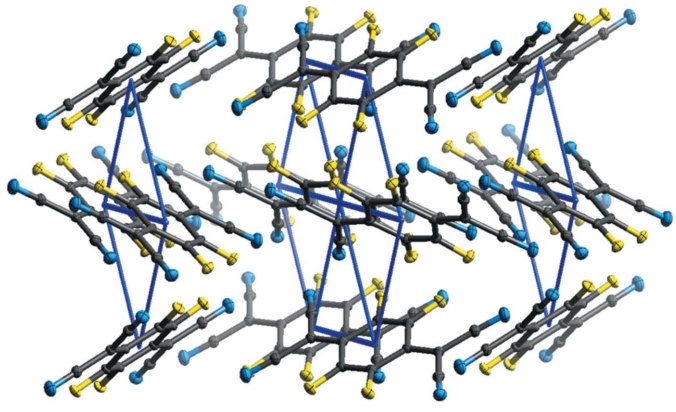

Figure 14
Energy framework of F_4TCNQ polymorph I, calculated using *CrystalExplorer17.5* (with pairwise energies < 15 kJ mol^{-1} removed for clarity).

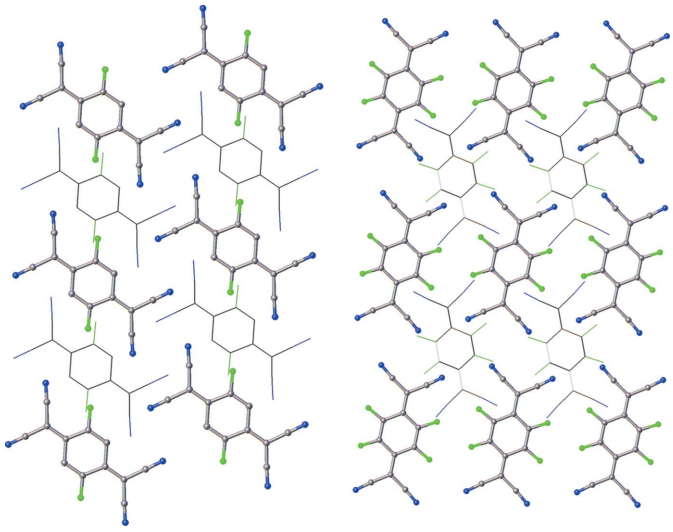

Figure 15
Views of F_2TCNQ along the [010] axis (left) and of F_4TCNQ along the [010] axis (right). In F_2TCNQ, molecules in adjacent layers (drawn with wireframe model) are in the same direction, which is not the case in F_4TCNQ.

between the solvent and the molecule which prohibits or makes it less favourable to form the polymorph II. This may be the result of an interaction between the cyano group of acetonitrile with the C—F bond of F_4TCNQ. A similar ring formed of these interactions is seen between acetonitrile and a C—F moiety in hexakis(pentafluorophenyl)[28]hexaphyrin (LIVHUV; Ishida *et al.*, 2014). If acetonitrile blocks other molecules of F_4TCNQ from associating with the C—F bond to form the stabilizing four-membered ring close contact motif by interacting in that position itself, then other interactions may take precedent during crystallization to direct the formation of the structure. If this is indeed the case, then polymorph II is able to form in DCM as the cyano group is absent from the solvent.

3.5. Comparison of polymorph II to F_2TCNQ

The reported structure of F_2TCNQ (Krupskaya *et al.*, 2015) was analysed in a similar way to the polymorphs of F_4TCNQ.

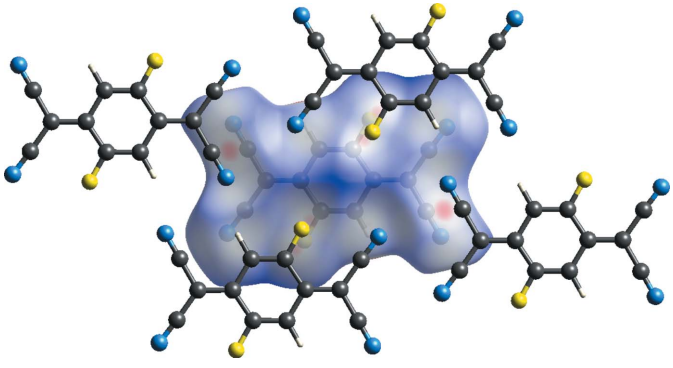

Figure 16
Hirshfeld surface of F_2TCNQ, showing the close contacts between layers, with adjacent molecules shown.

The layered arrangement of molecules in F_2TCNQ (Fig. 2) is similar to F_4TCNQ polymorph II, with layers at a distance of 2.9275 (2) Å with respect to each other. The main difference between F_2TCNQ and polymorph II is a change in the orientation of the molecules in adjacent layers (Fig. 15). This change in orientation precludes the formation of the four-membered C≡N···C—F close contact ring motif observed in polymorph II. Instead, as seen in the Hirshfeld surface (Fig. 16), a C—F···C—F four-membered close contact motif is formed. A similar four-membered ring of close contacts is also seen between two cyano groups in adjacent layers in this structure. As F_2TCNQ contains H atoms, hydrogen bonds can and do form, with C—H···N≡C contacts forming between the molecules within layers.

Pairwise interaction energies were calculated for CSD refcode BERZON03 (Krupskaya *et al.*, 2015; Table S4 in the supporting information). There are two different interacting modes between molecules in adjacent layers to a central molecule, unlike in polymorph II where there is only one. Similarly, there are two types of interaction to the central molecule from molecules in the same layer – one set of molecules that forms hydrogen bonds and another which has no close contacts; these are coloured in Fig. S13 (see supporting information).

Like polymorph II, the largest pairwise interaction energy is calculated between molecules in adjacent layers to the molecule with a C—F four-membered ring motif and a C—H···N close contact. This value is smaller than the inter-layer interaction of polymorph II (−29.0 *versus* 33.0 kJ mol^{-1}). The calculated energy of dispersion in this pair is larger than in polymorph II; however, the electrostatic energy is much smaller. Molecules that form close contacts to hydrogen, found within the layers, give the next largest value (−26.4 kJ mol^{-1}). The smallest value corresponds to the other molecule within the layer, which forms no close contacts to the central molecule. The average energy for the surrounding interactions to the central molecule is calculated as −21.0 kJ mol^{-1}.

3.6. Structure of F_4TCNQ–toluene solvate

The F_4TCNQ and toluene molecules lie in layers perpendicular to the [101] direction; further details are in the supporting information (§S3).

4. Summary

The results reported here provide a clear example of polymorphism in F_4TCNQ. A second polymorph of F4TCNQ, polymorph II, was grown concomitantly alongside the previously known polymorph I from a saturated solution of DCM. Pairwise interaction energies calculated in *CrystalExplorer* show that both structures have similar total energies – with polymorph II being the lowest, suggesting that polymorph II may be the more thermodynamic polymorph. Polymorph II exhibits a layered structure, with one molecule in the reduced unit cell, which has been suggested to promote

electron mobility and charge transfer (Chernyshov *et al.*, 2017). The structure is also very similar to the reported structure of F_2TCNQ, which does possess such properties. Further study of this polymorph could provide new insights into charge mobility in this family of compounds.

Funding information

Funding for this research was provided by: Engineering and Physical Sciences Research Council (EPSRC) (award reference 1663905); Newcastle University.

References

Alvarez, S. (2013). *Dalton Trans.* **42**, 8617–8636.
Bernstein, J. (1993). *J. Phys. D Appl. Phys.* **26**, B66–B76.
Bernstein, J. & Bernstein, J. M. (2002). In *Polymorphism in Molecular Crystals*. London: Clarendon Press.
Bruker (2009). *APEX2*, *SAINT* and *XPREP*. Bruker AXS Inc., Madison, Wisconsin, USA.
Bruker (2016). *SADABS*. Bruker AXS Inc., Madison, Wisconsin, USA.
Chernyshov, I. Yu., Vener, M. V., Feldman, E. V., Paraschuk, D. Yu. & Sosorev, A. Yu. (2017). *J. Phys. Chem. Lett.* **8**, 2875–2880.
Clark, R. C. & Reid, J. S. (1995). *Acta Cryst.* A**51**, 887–897.
Cochran, J. E., Junk, M. J. N., Glaudell, A. M., Miller, P. L., Cowart, J. S., Toney, M. F., Hawker, C. J., Chmelka, B. F. & Chabinyc, M. L. (2014). *Macromolecules*, **47**, 6836–6846.
Coropceanu, V., Cornil, J., da Silva Filho, D. A., Olivier, Y., Silbey, R. & Brédas, J.-L. (2007). *Chem. Rev.* **107**, 926–952.
Dolomanov, O. V., Bourhis, L. J., Gildea, R. J., Howard, J. A. K. & Puschmann, H. (2009). *J. Appl. Cryst.* **42**, 339–341.
Emge, T. J., Maxfield, M., Cowan, D. O. & Kistenmacher, T. J. (1981). *Mol. Cryst. Liq. Cryst.* **65**, 161–178.
Fan, G. & Yan, D. (2014). *Sci. Rep.* **4**, 1–8.
Fratini, S., Mayou, D. & Ciuchi, S. (2016). *Adv. Funct. Mater.* **26**, 2292–2315.
Fujii, T. & Yamakado, H. (2018). *IUCrData*, **3**, x180077.
Gao, W. & Kahn, A. (2001). *Appl. Phys. Lett.* **79**, 4040–4042.
Groom, C. R., Bruno, I. J., Lightfoot, M. P. & Ward, S. C. (2016). *Acta Cryst.* B**72**, 171–179.
Hu, P., Li, H., Li, Y., Jiang, H. & Kloc, C. (2017). *CrystEngComm*, **19**, 618–624.
Isakov, A. I., Kotelnikova, E. N., Kryuchkova, L. Y. & Lorenz, H. (2013). *Trans. Tianjin Univ.* **19**, 86–91.
Ishida, S., Higashino, T., Mori, S., Mori, H., Aratani, N., Tanaka, T., Lim, J. M., Kim, D. & Osuka, A. (2014). *Angew. Chem. Int. Ed.* **53**, 3427–3431.
Ji, L.-F., Fan, J.-X., Zhang, S.-F. & Ren, A.-M. (2018). *Phys. Chem. Chem. Phys.* **20**, 3784–3794.
Krupskaya, Y., Gibertini, M., Marzari, N. & Morpurgo, A. F. (2015). *Adv. Mater.* **27**, 2453–2458.
Macchi, P., Bürgi, H.-B., Chimpri, A. S., Hauser, J. & Gál, Z. (2011). *J. Appl. Cryst.* **44**, 763–771.
Macrae, C. F., Sovago, I., Cottrell, S. J., Galek, P. T. A., McCabe, P., Pidcock, E., Platings, M., Shields, G. P., Stevens, J. S., Towler, M. & Wood, P. A. (2020). *J. Appl. Cryst.* **53**, 226–235.
McKinnon, J. J., Jayatilaka, D. & Spackman, M. A. (2007). *Chem. Commun.* pp. 3814–3818.
Metrangolo, P. & Resnati, G. (2014). *IUCrJ*, **1**, 5–7.
Pingel, P., Schwarzl, R. & Neher, D. (2012). *Appl. Phys. Lett.* **100**, 143303.
Rigaku OD (2015). *CrysAlis PRO*. Rigaku Oxford Diffraction Ltd, Yarnton, Oxfordshire, England.
Salzillo, T., Masino, M., Kociok-Köhn, G., Di Nuzzo, D., Venuti, E., Della Valle, R. G., Vanossi, D., Fontanesi, C., Girlando, A., Brillante, A. & Da Como, E. (2016). *Cryst. Growth Des.* **16**, 3028–3036.
Sheldrick, G. M. (2015*a*). *Acta Cryst.* A**71**, 3–8.
Sheldrick, G. M. (2015*b*). *Acta Cryst.* C**71**, 3–8.
Shukla, R., Ruzié, C., Schweicher, G., Kennedy, A. R., Geerts, Y. H., Chopra, D. & Chattopadhyay, B. (2019). *Acta Cryst.* B**75**, 71–78.
Sosorev, A. Y. (2017). *Phys. Chem. Chem. Phys.* **19**, 25478–25486.
Sosorev, A. Y., Chernyshov, I. Y., Paraschuk, D. Y. & Vener, M. V. (2019). *Molecular Spectroscopy*, pp. 425–458. Chichester: John Wiley & Sons Ltd.
Sosorev, A. Y., Maslennikov, D. R., Chernyshov, I. Y., Dominskiy, D. I., Bruevich, V. V., Vener, M. V. & Paraschuk, D. Y. (2018). *Phys. Chem. Chem. Phys.* **20**, 18912–18918.
Spackman, M. A. & Jayatilaka, D. (2009). *CrystEngComm*, **11**, 19–32.
Spackman, M. A. & McKinnon, J. J. (2002). *CrystEngComm*, **4**, 378–392.
Storm, A., Michaelsen, C., Oehr, A. & Hoffmann, C. (2004). *Proc. SPIE*, **5537**, 177–182.
Sutton, A. L., Abrahams, B. F., D'Alessandro, D. M., Hudson, T. A., Robson, R. & Usov, P. M. (2016). *CrystEngComm*, **18**, 8906–8914.
Tran, T. T.-D., Tran, P. H.-L., Park, J.-B. & Lee, B.-J. (2012). *Arch. Pharm. Res.* **35**, 1223–1230.
Turner, M. J., Grabowsky, S., Jayatilaka, D. & Spackman, M. A. (2014). *J. Phys. Chem. Lett.* **5**, 4249–4255.
Turner, M. J., McKinnon, J. J., Wolff, S. K., Grimwood, D. J., Spackman, P. R., Jayatilaka, D. & Spackman, M. A. (2017). *CrystalExplorer17*. University of Western Australia. https://crystalexplorer.scb.uwa.edu.au/.
Wang, C., Dong, H., Hu, W., Liu, Y. & Zhu, D. (2012). *Chem. Rev.* **112**, 2208–2267.
Wiscons, R. A., Goud, N. R., Damron, J. T. & Matzger, A. J. (2018). *Angew. Chem. Int. Ed.* **57**, 9044–9047.

supporting information

Acta Cryst. (2021). C**77**, 426-434 [https://doi.org/10.1107/S2053229621006252]

Structural investigations into a new polymorph of F_4TCNQ: towards enhanced semiconductor properties

Natalie T. Johnson, Michael R. Probert and Paul G. Waddell

Computing details

Data collection: *APEX2* (Bruker, 2009) for polymorph_i, polymorph_ii; *CrysAlis PRO* (Rigaku OD, 2015) for toluene_solvate. Cell refinement: *SAINT* (Bruker, 2009) for polymorph_i, polymorph_ii; *CrysAlis PRO* (Rigaku OD, 2015) for toluene_solvate. Data reduction: *SAINT* (Bruker, 2009) for polymorph_i, polymorph_ii; *CrysAlis PRO* (Rigaku OD, 2015) for toluene_solvate. For all structures, program(s) used to solve structure: SHELXT (Sheldrick, 2015a); program(s) used to refine structure: *SHELXL2014* (Sheldrick, 2015b); molecular graphics: OLEX2 (Dolomanov *et al.*, 2009). Software used to prepare material for publication: OLEX2 (Dolomanov *et al.*, 2009) and *XPREP* (Bruker, 2009) for polymorph_i, polymorph_ii; OLEX2 (Dolomanov *et al.*, 2009) for toluene_solvate.

2-[4-(Dicyanomethylidene)-2,3,5,6-tetrafluorocyclohexa-2,5-dien-1-ylidene]propanedinitrile (polymorph_i)

Crystal data

$C_{12}F_4N_4$
M_r = 276.16
Orthorhombic, *Pbca*
a = 9.1799 (3) Å
b = 8.0482 (3) Å
c = 14.5541 (5) Å
V = 1075.28 (6) Å^3
Z = 4
F(000) = 544
D_x = 1.706 Mg m^{-3}
Ag $K\alpha$ radiation, λ = 0.56086 Å
Cell parameters from 9611 reflections
θ = 2.9–35.1°
μ = 0.09 mm^{-1}
T = 100 K
Cube, yellow
0.28 × 0.22 × 0.16 mm

Data collection

Bruker Photon II CPAD diffractometer
Multi-layer optics monochromator
φ and ω scans
Absorption correction: numerical (SADABS; Bruker, 2016)
T_{min} = 0.919, T_{max} = 0.982
189710 measured reflections
5103 independent reflections
4271 reflections with $I > 2\sigma(I)$
R_{int} = 0.043
θ_{max} = 35.8°, θ_{min} = 2.8°
h = −19→19
k = −16→16
l = −30→30

Refinement

Refinement on F^2
Least-squares matrix: full
$R[F^2 > 2\sigma(F^2)]$ = 0.034
$wR(F^2)$ = 0.115
S = 1.09
5103 reflections
91 parameters
0 restraints
$w = 1/[\sigma^2(F_o^2) + (0.0599P)^2 + 0.1298P]$ where $P = (F_o^2 + 2F_c^2)/3$

$(\Delta/\sigma)_{max}$ = 0.001
$\Delta\rho_{max}$ = 0.75 e Å^{-3}
$\Delta\rho_{min}$ = −0.33 e Å^{-3}

Special details

Geometry. All esds (except the esd in the dihedral angle between two l.s. planes) are estimated using the full covariance matrix. The cell esds are taken into account individually in the estimation of esds in distances, angles and torsion angles; correlations between esds in cell parameters are only used when they are defined by crystal symmetry. An approximate (isotropic) treatment of cell esds is used for estimating esds involving l.s. planes.

Refinement. Integration was performed using *SAINT* (Bruker, 2012) with a 0.48 Å cut-off, default integration algorithm and best-plane background. The data were scaled and merged in *SADABS* using the default error model (Bruker, 2001); a correction for overloaded reflections and a numerical absorption correction based on the faces of the crystal were applied. The space group was identified in *XPREP* (Bruker, 2012) and the solution and refinement were performed in the *OLEX2* GUI (Dolomanov *et al.*, 2009) using *XT* and *XL*, respectively (Bruker, 2012).

Fractional atomic coordinates and isotropic or equivalent isotropic displacement parameters (Å^2)

	x	*y*	*z*	U_{iso}*/U_{eq}
F1	0.34119 (3)	0.73648 (4)	0.55965 (2)	0.01881 (6)
F2	0.65038 (4)	0.99400 (4)	0.33962 (2)	0.01955 (6)
N1	0.34397 (5)	0.44491 (6)	0.42766 (3)	0.02166 (7)
N2	0.61198 (6)	0.67225 (7)	0.23109 (3)	0.02644 (9)
C1	0.41948 (4)	0.86469 (5)	0.53012 (3)	0.01461 (6)
C2	0.57501 (4)	0.99735 (5)	0.41743 (3)	0.01464 (6)
C3	0.49248 (4)	0.85233 (5)	0.44277 (3)	0.01399 (6)
C4	0.48306 (4)	0.71426 (5)	0.38721 (3)	0.01542 (6)
C5	0.40263 (5)	0.56860 (6)	0.41153 (3)	0.01741 (7)
C6	0.55569 (5)	0.69859 (6)	0.30068 (3)	0.01875 (7)

Atomic displacement parameters (Å^2)

	U^{11}	U^{22}	U^{33}	U^{12}	U^{13}	U^{23}
F1	0.01913 (11)	0.01634 (11)	0.02097 (12)	−0.00341 (8)	0.00560 (8)	0.00344 (8)
F2	0.02069 (12)	0.02078 (12)	0.01719 (11)	−0.00031 (9)	0.00806 (9)	0.00220 (8)
N1	0.02127 (16)	0.01929 (15)	0.02442 (16)	−0.00355 (12)	0.00067 (12)	−0.00021 (12)
N2	0.0318 (2)	0.0309 (2)	0.01659 (14)	−0.00044 (17)	0.00326 (14)	−0.00232 (13)
C1	0.01318 (12)	0.01527 (12)	0.01537 (12)	−0.00081 (9)	0.00210 (9)	0.00315 (9)
C2	0.01350 (12)	0.01625 (13)	0.01416 (12)	0.00000 (9)	0.00261 (9)	0.00293 (9)
C3	0.01220 (11)	0.01563 (12)	0.01415 (12)	0.00033 (9)	0.00071 (9)	0.00261 (9)
C4	0.01433 (13)	0.01705 (13)	0.01488 (12)	−0.00006 (10)	−0.00045 (9)	0.00163 (10)
C5	0.01608 (14)	0.01779 (14)	0.01836 (14)	−0.00126 (11)	−0.00094 (11)	0.00064 (11)
C6	0.01994 (16)	0.02142 (16)	0.01489 (13)	−0.00005 (12)	−0.00028 (11)	0.00013 (11)

Geometric parameters (Å, º)

F1—C1	1.3289 (5)	C1—C3	1.4405 (5)
F2—C2	1.3274 (5)	C2—C3	1.4395 (5)
N1—C5	1.1559 (6)	C3—C4	1.3771 (6)
N2—C6	1.1566 (6)	C4—C5	1.4299 (6)
C1—C2^{i}	1.3484 (6)	C4—C6	1.4305 (6)

F1—C1—C2^{i}	118.46 (3)	C4—C3—C1	123.01 (4)
F1—C1—C3	118.91 (4)	C4—C3—C2	122.47 (4)
C2^{i}—C1—C3	122.62 (3)	C3—C4—C5	123.28 (4)
F2—C2—C1^{i}	118.69 (4)	C3—C4—C6	123.97 (4)
F2—C2—C3	118.45 (4)	C5—C4—C6	112.72 (4)
C1^{i}—C2—C3	122.85 (3)	N1—C5—C4	175.48 (5)
C2—C3—C1	114.52 (4)	N2—C6—C4	174.43 (6)

Symmetry code: (i) −*x*+1, −*y*+2, −*z*+1.

2-[4-(Dicyanomethylidene)-2,3,5,6-tetrafluorocyclohexa-2,5-dien-1-ylidene]propanedinitrile (polymorph_ii)

Crystal data

$C_{12}F_4N_4$
M_r = 276.16
Orthorhombic, *Pnnm*
a = 7.5140 (4) Å
b = 11.6787 (6) Å
c = 5.9347 (3) Å
V = 520.79 (5) Å^3
Z = 2
F(000) = 272
D_x = 1.761 Mg m^{-3}
Ag *Kα* radiation, *λ* = 0.56086 Å
Cell parameters from 9821 reflections
θ = 2.5–35.7°
μ = 0.10 mm^{-1}
T = 100 K
Octahedral, yellow
0.3 × 0.17 × 0.12 mm

Data collection

Bruker Photon II CPAD diffractometer
Multi-layer optics monochromator
φ and *ω* scans
Absorption correction: numerical (SADABS; Bruker, 2016)
T_{min} = 0.931, T_{max} = 0.974
115983 measured reflections
2628 independent reflections
2285 reflections with $I > 2\sigma(I)$
R_{int} = 0.043
θ_{max} = 35.8°, θ_{min} = 2.5°
h = −15→15
k = −24→24
l = −12→12

Refinement

Refinement on F^2
Least-squares matrix: full
$R[F^2 > 2\sigma(F^2)]$ = 0.031
$wR(F^2)$ = 0.111
S = 1.07
2628 reflections
61 parameters
0 restraints
$w = 1/[\sigma^2(F_o^2) + (0.0647P)^2 + 0.0518P]$ where $P = (F_o^2 + 2F_c^2)/3$
$(\Delta/\sigma)_{max}$ = 0.001
$\Delta\rho_{max}$ = 0.77 e Å^{-3}
$\Delta\rho_{min}$ = −0.26 e Å^{-3}

Special details

Geometry. All esds (except the esd in the dihedral angle between two l.s. planes) are estimated using the full covariance matrix. The cell esds are taken into account individually in the estimation of esds in distances, angles and torsion angles; correlations between esds in cell parameters are only used when they are defined by crystal symmetry. An approximate (isotropic) treatment of cell esds is used for estimating esds involving l.s. planes.

Refinement. Integration was performed using *SAINT* (Bruker, 2012) with a 0.48 Å cut-off, default integration algorithm and best-plane background. The data were scaled and merged in *SADABS* using the default error model (Bruker, 2001); a correction for overloaded reflections and a numerical absorption correction based on the faces of the crystal were applied. The space group was identified in *XPREP* (Bruker, 2012) and the solution and refinement were performed in the *OLEX2* GUI (Dolomanov *et al.*, 2009) using *XT* and *XL*, respectively (Bruker, 2012).

Fractional atomic coordinates and isotropic or equivalent isotropic displacement parameters (Å²)

	x	*y*	*z*	U_{iso}*/U_{eq}
F1	0.84334 (4)	0.57162 (3)	0.500000	0.01752 (7)
F2	0.22159 (4)	0.64847 (3)	0.500000	0.01705 (7)
N1	0.88414 (7)	0.82906 (5)	0.500000	0.02014 (9)
N2	0.33496 (8)	0.89850 (5)	0.500000	0.02405 (11)
C1	0.67562 (6)	0.53722 (4)	0.500000	0.01313 (7)
C2	0.35867 (6)	0.57628 (4)	0.500000	0.01324 (7)
C3	0.53646 (6)	0.62208 (4)	0.500000	0.01262 (7)
C4	0.57115 (6)	0.73787 (4)	0.500000	0.01376 (7)
C5	0.74684 (7)	0.78452 (5)	0.500000	0.01551 (8)
C6	0.43587 (7)	0.82395 (4)	0.500000	0.01695 (8)

Atomic displacement parameters (Å²)

	U^{11}	U^{22}	U^{33}	U^{12}	U^{13}	U^{23}
F1	0.00841 (11)	0.01994 (14)	0.02420 (16)	−0.00123 (9)	0.000	0.000
F2	0.01019 (11)	0.01795 (13)	0.02302 (15)	0.00334 (9)	0.000	0.000
N1	0.01638 (17)	0.0230 (2)	0.02105 (19)	−0.00510 (14)	0.000	0.000
N2	0.0207 (2)	0.01925 (19)	0.0322 (3)	0.00476 (15)	0.000	0.000
C1	0.00854 (13)	0.01638 (16)	0.01447 (15)	0.00000 (11)	0.000	0.000
C2	0.00917 (13)	0.01611 (15)	0.01445 (15)	0.00121 (11)	0.000	0.000
C3	0.00982 (13)	0.01572 (15)	0.01233 (14)	0.00027 (11)	0.000	0.000
C4	0.01195 (14)	0.01585 (16)	0.01347 (15)	0.00005 (11)	0.000	0.000
C5	0.01391 (15)	0.01821 (17)	0.01441 (15)	−0.00209 (13)	0.000	0.000
C6	0.01531 (17)	0.01650 (17)	0.01903 (18)	0.00100 (13)	0.000	0.000

Geometric parameters (Å, º)

F1—C1	1.3227 (5)	C1—C3	1.4407 (6)
F2—C2	1.3310 (6)	C2—C3	1.4390 (6)
N1—C5	1.1554 (7)	C3—C4	1.3772 (7)
N2—C6	1.1545 (8)	C4—C5	1.4281 (7)
C1—C2^{i}	1.3503 (7)	C4—C6	1.4296 (7)
F1—C1—C2^{i}	118.68 (4)	C4—C3—C1	122.55 (4)
F1—C1—C3	118.86 (4)	C4—C3—C2	122.73 (4)
C2^{i}—C1—C3	122.47 (4)	C3—C4—C5	123.34 (5)
F2—C2—C1^{i}	118.30 (4)	C3—C4—C6	123.77 (5)
F2—C2—C3	118.88 (4)	C5—C4—C6	112.90 (5)
C1^{i}—C2—C3	122.82 (4)	N1—C5—C4	175.67 (6)
C2—C3—C1	114.71 (4)	N2—C6—C4	175.73 (6)

Symmetry code: (i) −*x*+1, −*y*+1, −*z*+1.

2-[4-(Dicyanomethylidene)-2,3,5,6-tetrafluorocyclohexa-2,5-dien-1-ylidene]propanedinitrile toluene monosolvate (toluene_solvate)

Crystal data

$C_{12}F_4N_4·C_7H_8$
M_r = 368.29
Monoclinic, $P2_1/c$
a = 8.1314 (2) Å
b = 7.4141 (2) Å
c = 13.6796 (4) Å
β = 100.551 (3)°
V = 810.76 (4) Å^3
Z = 2
$F(000)$ = 372
D_x = 1.509 Mg m^{-3}
Cu $K\alpha$ radiation, λ = 1.54184 Å
Cell parameters from 3336 reflections
θ = 5.5–66.3°
μ = 1.09 mm^{-1}
T = 150 K
Needle, red
0.41 × 0.05 × 0.03 mm

Data collection

Rigaku Xcalibur Atlas Gemini ultra diffractometer
Radiation source: fine-focus sealed X-ray tube, Enhance Ultra (Cu) X-ray Source
Mirror monochromator
Detector resolution: 10.3968 pixels mm^{-1}
ω scans
Absorption correction: analytical [CrysAlis PRO (Rigaku OD, 2015), based on expressions derived by Clark & Reid (1995)]
T_{min} = 0.806, T_{max} = 0.975
10970 measured reflections
1433 independent reflections
1194 reflections with $I > 2\sigma(I)$
R_{int} = 0.045
θ_{max} = 66.9°, θ_{min} = 5.5°
h = −9→9
k = −8→8
l = −16→16

Refinement

Refinement on F^2
Least-squares matrix: full
$R[F^2 > 2\sigma(F^2)]$ = 0.039
$wR(F^2)$ = 0.109
S = 1.08
1433 reflections
155 parameters
161 restraints
Primary atom site location: dual
Hydrogen site location: inferred from neighbouring sites
H-atom parameters constrained
$w = 1/[\sigma^2(F_o^2) + (0.0549P)^2 + 0.3028P]$ where $P = (F_o^2 + 2F_c^2)/3$
$(\Delta/\sigma)_{max}$ = 0.001
$\Delta\rho_{max}$ = 0.44 e Å^{-3}
$\Delta\rho_{min}$ = −0.21 e Å^{-3}

Special details

Geometry. All esds (except the esd in the dihedral angle between two l.s. planes) are estimated using the full covariance matrix. The cell esds are taken into account individually in the estimation of esds in distances, angles and torsion angles; correlations between esds in cell parameters are only used when they are defined by crystal symmetry. An approximate (isotropic) treatment of cell esds is used for estimating esds involving l.s. planes.

Refinement. The structure of the F_4TCNQ–toluene solvate has half a molecule of solvent in the asymmetric unit. The toluene molecule was modelled as disordered over two sites across a centre of symmetry. The occupancies of the two parts were constrained to be 0.5 and the atomic displacement parameters were restrained. The geometry of the toluene molecule was restrained.

Diffraction frames for the F_4TCNQ–toluene solvate crystal were integrated and scaled using *CrysAlis PRO* (Rigaku OD, 2006). Intensities were corrected for absorption using a multifaceted crystal model created by indexing the faces of the crystal for which data were collected (Clark & Reid, 1995). The structure solution and refinement were performed using *XL* and *XT* respectively within the *OLEX2* GUI.

Fractional atomic coordinates and isotropic or equivalent isotropic displacement parameters (Å²)

	x	*y*	*z*	U_{iso}*/U_{eq}	Occ. (<1)
F1	0.43765 (13)	0.77387 (14)	0.62015 (7)	0.0346 (3)	
F2	0.40784 (14)	0.15463 (14)	0.52795 (7)	0.0350 (3)	
N1	0.2912 (2)	0.6437 (2)	0.79955 (11)	0.0415 (4)	
N2	0.2643 (2)	0.1032 (2)	0.71642 (13)	0.0463 (5)	
C1	0.41901 (19)	0.4595 (2)	0.58369 (11)	0.0261 (4)	
C2	0.4694 (2)	0.6385 (2)	0.56168 (12)	0.0269 (4)	
C3	0.4539 (2)	0.3239 (2)	0.51478 (12)	0.0271 (4)	
C4	0.3476 (2)	0.4196 (2)	0.66478 (12)	0.0288 (4)	
C5	0.3167 (2)	0.5505 (3)	0.73712 (12)	0.0318 (4)	
C6	0.3012 (2)	0.2405 (3)	0.68933 (13)	0.0333 (4)	
C7	−0.017 (3)	0.6337 (18)	0.5496 (11)	0.041 (2)	0.5
C8	0.0532 (18)	0.6483 (18)	0.4627 (8)	0.033 (2)	0.5
H8	0.0900	0.7594	0.4435	0.039*	0.5
C9	0.066 (2)	0.4980 (17)	0.4072 (11)	0.036 (2)	0.5
H9	0.1131	0.5074	0.3504	0.044*	0.5
C10	0.012 (2)	0.3361 (18)	0.4329 (10)	0.038 (2)	0.5
H10	0.0195	0.2367	0.3924	0.045*	0.5
C11	−0.052 (2)	0.3156 (18)	0.5158 (9)	0.035 (2)	0.5
H11	−0.0860	0.2020	0.5329	0.042*	0.5
C12	−0.068 (2)	0.4606 (15)	0.5758 (10)	0.032 (2)	0.5
H12	−0.1117	0.4451	0.6334	0.039*	0.5
C13	−0.0309 (7)	0.8049 (7)	0.6121 (4)	0.0565 (12)	0.5
H13A	0.0563	0.8879	0.6042	0.085*	0.5
H13B	−0.0200	0.7725	0.6809	0.085*	0.5
H13C	−0.1378	0.8606	0.5899	0.085*	0.5

Atomic displacement parameters (Å²)

	U^{11}	U^{22}	U^{33}	U^{12}	U^{13}	U^{23}
F1	0.0471 (6)	0.0294 (6)	0.0307 (5)	0.0035 (4)	0.0160 (4)	−0.0051 (4)
F2	0.0464 (6)	0.0256 (5)	0.0364 (5)	−0.0011 (4)	0.0167 (5)	0.0014 (4)
N1	0.0469 (10)	0.0491 (10)	0.0316 (8)	0.0035 (8)	0.0156 (7)	−0.0036 (7)
N2	0.0561 (11)	0.0425 (10)	0.0463 (9)	0.0016 (8)	0.0247 (8)	0.0084 (8)
C1	0.0238 (8)	0.0307 (9)	0.0238 (8)	0.0039 (7)	0.0046 (6)	0.0010 (6)
C2	0.0290 (8)	0.0273 (9)	0.0249 (8)	0.0053 (7)	0.0062 (6)	−0.0017 (7)
C3	0.0284 (9)	0.0254 (9)	0.0278 (8)	0.0024 (7)	0.0060 (6)	0.0019 (6)
C4	0.0275 (9)	0.0346 (9)	0.0252 (8)	0.0053 (7)	0.0068 (6)	0.0036 (7)
C5	0.0307 (9)	0.0391 (10)	0.0272 (8)	0.0022 (8)	0.0092 (7)	0.0042 (7)
C6	0.0338 (10)	0.0391 (11)	0.0294 (9)	0.0043 (8)	0.0122 (7)	0.0030 (8)
C7	0.036 (3)	0.049 (4)	0.037 (5)	0.009 (3)	0.001 (4)	−0.012 (3)
C8	0.031 (3)	0.038 (6)	0.030 (5)	0.003 (4)	0.008 (3)	0.000 (3)
C9	0.029 (3)	0.059 (5)	0.023 (4)	0.013 (4)	0.010 (3)	−0.006 (3)
C10	0.032 (3)	0.050 (4)	0.030 (4)	0.016 (3)	0.001 (3)	−0.018 (3)
C11	0.036 (3)	0.032 (4)	0.034 (4)	0.008 (3)	0.000 (3)	−0.005 (3)
C12	0.030 (3)	0.049 (5)	0.020 (5)	0.007 (4)	0.010 (3)	−0.004 (3)

C13	0.053 (3)	0.056 (3)	0.060 (3)	0.001 (2)	0.008 (2)	−0.010 (2)

Geometric parameters (Å, º)

F1—C2	1.3375 (19)	C4—C5	1.441 (3)
F2—C3	1.332 (2)	C4—C6	1.437 (3)
N1—C5	1.147 (2)	C7—C8	1.414 (9)
N2—C6	1.142 (3)	C7—C12	1.414 (10)
C1—C2	1.438 (3)	C7—C13	1.546 (10)
C1—C3	1.441 (2)	C8—C9	1.364 (8)
C1—C4	1.375 (2)	C9—C10	1.346 (10)
C2—C3^{i}	1.341 (2)	C10—C11	1.342 (9)
C3—C2^{i}	1.341 (2)	C11—C12	1.372 (8)
C2—C1—C3	114.15 (15)	C6—C4—C5	112.08 (14)
C4—C1—C2	123.11 (16)	N1—C5—C4	174.69 (19)
C4—C1—C3	122.72 (16)	N2—C6—C4	174.48 (19)
F1—C2—C1	118.28 (14)	C8—C7—C12	117.6 (8)
F1—C2—C3^{i}	118.62 (16)	C8—C7—C13	118.9 (8)
C3^{i}—C2—C1	123.10 (16)	C12—C7—C13	123.4 (8)
F2—C3—C1	118.35 (14)	C9—C8—C7	119.3 (9)
F2—C3—C2^{i}	118.91 (15)	C10—C9—C8	121.5 (9)
C2^{i}—C3—C1	122.73 (16)	C11—C10—C9	121.1 (9)
C1—C4—C5	124.16 (17)	C10—C11—C12	120.7 (9)
C1—C4—C6	123.71 (16)	C11—C12—C7	119.7 (9)

Symmetry code: (i) −*x*+1, −*y*+1, −*z*+1.